

RSC Advances



This is an *Accepted Manuscript*, which has been through the Royal Society of Chemistry peer review process and has been accepted for publication.

Accepted Manuscripts are published online shortly after acceptance, before technical editing, formatting and proof reading. Using this free service, authors can make their results available to the community, in citable form, before we publish the edited article. This *Accepted Manuscript* will be replaced by the edited, formatted and paginated article as soon as this is available.

You can find more information about *Accepted Manuscripts* in the [Information for Authors](#).

Please note that technical editing may introduce minor changes to the text and/or graphics, which may alter content. The journal's standard [Terms & Conditions](#) and the [Ethical guidelines](#) still apply. In no event shall the Royal Society of Chemistry be held responsible for any errors or omissions in this *Accepted Manuscript* or any consequences arising from the use of any information it contains.

ARTICLE

Electrodeposited p-type Co_3O_4 with high photoelectrochemical performance in aqueous medium

Cite this: DOI: 10.1039/x0xx00000x

M. Ebadi^a, M. A. Mat-Teridi^b, M. Y. Sulaiman^b, W. J. Basirun^c, N. Asim^b, N. A. Ludin^b, M. A. Ibrahim^b and K. Sopian^b

Received 00th January 2012,
Accepted 00th January 2012

DOI: 10.1039/x0xx00000x

www.rsc.org/

p-type Co_3O_4 photocathodes with different amount of CuO, were synthesized on fluorine doped tin oxide (FTO) via electrodeposition from chloride bath containing suspended starch particles. All of the fabricated samples were photoresponsive toward water splitting in 0.5 M Na_2SO_4 under simulated sunlight. The PEC performance was evaluated using LSPV, Chronoamperometry, and EIS techniques. The samples fabricated via the electrodeposition/anodizing/annealing process showed greater photocurrent response compared to electrodeposition/annealing process. Among all, the sample with an atomic composition % of Co: 24.9, Cu: 25.0 and O: 50.1 showed an optimum photocurrent response ($\sim 6.5 \text{ mA cm}^{-2}$ vs SCE at -0.3 V). The structure, morphology/composition and optical response were characterized by XRD, FESEM/EDX and UV-Vis techniques, respectively.

1. Introduction

Photoelectrochemical (PEC) water splitting is a promising route for the clean generation of hydrogen fuel and oxygen. However the search for materials with a proper band-gap (\geq redox potential of water 1.23 eV) is a challenging task. Materials with semiconducting behavior are reported to exhibit photo responsive behavior toward water splitting due to the presence of an energy band-gap.¹⁻³ Among the different types of semiconductors such as nitrides, sulfides, phosphides, selenides and tellurides, metal oxides have better stability in aqueous solution in a wide range of pH. Furthermore, a reasonable photocurrent density can be obtained from a metal oxide with a band-gap close to 1.23 V. The metal oxides with n-type and p-type behavior have been extensively investigated for water splitting applications as photoanodes and photocathodes, respectively. One of the most important metal oxides is cobalt oxide which has been used in super capacitors, biosensors, lithium batteries and photoelectrochemical devices.⁴⁻⁶ Numerous researchers have reported a wide range of band-gap values for p-type cobalt oxides with different structures (1.37-2.7 eV).^{6,7}

Cobalt oxide has been fabricated by physical and chemical methods such as: hydrothermal, CVD, AACVD, electrophoretic and Electrodeposition/annealing.⁸⁻¹¹ However, the main limitation of cobalt oxide in solar driven water splitting is the energy consumption through the additional bias voltage. This drawback can be compensated once co-catalysts with a lower band gap (e.g. CuO; \sim

1.3 eV) are added to the cobalt oxide thin films. Recently, due to the lower cost and appropriate band-gap of copper oxide, it has been used as a highly effective semiconductor electrode in photoelectrochemical water splitting (PEC). However, pure copper oxide has lower stability unless mixed with other stable materials.^{12,13} Photocurrent response of metal oxides could be improved by increasing the active surface area through the fabrication of nano-sheets, mesopores, nanotubes and nanowires.⁵⁻¹⁴ In spite of the p-type behavior of Co_3O_4 , it has been mostly used as a catalyst and co-catalyst for the oxygen evolution reaction (OER), but only few studies on cobalt oxides were reported for the photoelectrochemical hydrogen evolution reaction (HER).¹⁵⁻¹⁷

In the present work, we have fabricated a number of Co_3O_4 -CuO thin films through the pulse-electrodeposition/anodization and annealing process. The thin films were obtained from cobalt and copper chlorides mixture of electrolytes (with suspended starch particles). The photoresponse and structural characterization of the fabricated films were also investigated.

1. Experimental methods

Electrode preparation: The fabrication of the p-type porous electrodes was performed using electrochemical and thermal techniques. The chemicals reagents (analytical grade) in this work were procured from Aldrich and used as received. Hierarchically, the

cobalt oxide thin films fabricated on the fluorine doped tin oxide (FTO) glass ($1 \times 1 \text{ cm}^2$) were prepared by the following steps:

i). The FTO glasses were ultrasonically cleaned in acetone for 7 min, rinsed in distilled water and dried in an oven. ii). the cobalt films (with different amount of copper) were electrodeposited on the FTO glass substrate, from a $\text{CoCl}_2 \cdot 6\text{H}_2\text{O} + \text{CuCl}_2 \cdot 2\text{H}_2\text{O}$ electrolyte at $\text{pH}=4$. A three compartment electrochemical cell with calomel as the reference electrode (RE), the fabricated thin films as the working electrode (WE) and a Pt mesh as the counter electrode (CE): were used in the electrochemical process. A potentiostat/ galvanostat from AutoLab, model PGSTAT 240 interfaced with a computer, were

used in this process. The layers were deposited using pulse chronoamperometry technique for 15 cycles with the following order, -10 mA cm^{-2} (10 s) and -6 mA cm^{-2} (5 s). The content of the electrolytes and the suspended starch (1.5 g l^{-1}) are tabulated in Table 1. ii). the same technique (chronoamperometry, $+10 \text{ mA cm}^{-2}$) was used for the anodization of the deposited layers in hydrogen peroxide (10%) for 10 min. iii). Finally the anodized layers were annealed in 500°C for 2 h in an open tube furnace to produce the Co_3O_4 and $\text{Co}_3\text{O}_4\text{-CuO}$ layers.

Table 1. The fabrication conditions during the electrodeposition/anodization/annealing process and elemental composition from EDX.

Sample Series	Sample Name	Electrodeposition			Anodization in (10% H_2O_2)	Annealing (500°C)	EDX / Atomic% (Co: Cu: O)
		$\text{CoCl}_2 \cdot 6\text{H}_2\text{O}$ (mM L^{-1})	$\text{CuCl}_2 \cdot 2\text{H}_2\text{O}$ (mM L^{-1})	Starch (1.5 g L^{-1})			
(I)	S_A	40	-	√	-	√	44: 0: 56
	S_B	40	5	√	-	√	33.9: 20.3: 45.8
	S_C	40	10	√	-	√	26.1: 27.3: 46.6
	S_D	40	20	√	-	√	12.8: 31.7: 55.5
(II)	* S_B	40	5	√	√	√	36.8: 18.4: 44.5
	* S_C	40	10	√	√	√	24.9: 25.0: 50.1
	* S_D	40	20	√	√	√	10.5: 29.7: 59.8
	* S_D'	40	20	√	√	-	13.1: 37.6: 47.3

Physical characterizations: The morphology and chemical composition of the photo-cathodes were investigated by field emission scanning electron microscopy (FESEM) and energy dispersive X-ray spectroscopy (EDX) (FESEM/EDX quanta 600), respectively. XRD (Bruker D_8 discover diffractometer with Cu K_α radiation, $\lambda=1.540598 \text{ \AA}$) was used to determine the crystalline structure of photo-cathodes. In addition, an UV-visible transmission spectrophotometer (Perkin Elmer lambda 650) was used to investigate the absorbance of the FTO coated samples using a bare FTO glass as the reference.

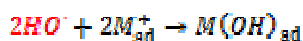
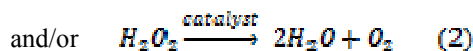
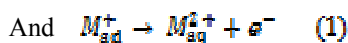
Photoelectrochemical (PEC) measurements: The PEC performance of the prepared cobalt oxide films was investigated in a photoelectrochemical cell with a quartz window (filled with $0.5 \text{ M Na}_2\text{SO}_4$). The PEC performance of the electrodes was measured in the dark and light illumination with a 150 W Xe lamp (100 mW cm^{-2}). The linear sweep photo-voltammetry (LSPV) was run at 5 mV s^{-1} between 0.3 to -0.6 V . Chronoamperometry at 0 V for 30 min was performed to examine the stability of the fabricated electrodes, using the same electrode configuration in the LSPV. The aforementioned

cell configuration and electrolyte were also used in the EIS measurements. The EIS measurements were performed at the open circuit potential condition with the V_{rms} of 10 mV and a frequency range between $100 \text{ kHz} - 10 \text{ mHz}$, using the frequency response analyzer (FRA) software installed in a computer and interfaced with the Autolab 240 potentiostat/ galvanostat. Alternatively, the Mott-Schottky plot were performed through the EIS technique at potential range (-0.2 to 0.3 V vs SCE) with frequencies of 10 , 1 and 0.1 kHz in the dark condition.

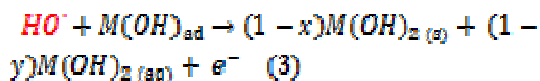
2. Results and discussions

The fabrication of the porous p-type semiconductor thin films was performed in the electrolytes with and without the starch suspension. The starch suspensions play an important role in the fabrication of the thin films. The numerous sites on the electrode surface were blocked by the starch particles, thus the nucleation and growth occurred on the free sites on the FTO substrate. Previous works have reported that porous thin films could be fabricated using *insitu* nanoparticles suspension which can be removed by chemical and

thermal process.¹⁸⁻²¹ In the fabrication process, the starch particles were removed from the thin film surface during the water rinsing and annealing (500°C) steps. During the penultimate process, the fabricated thin films were anodized in alkaline 10% hydrogen peroxide (pH=9) at +10 mV cm⁻² for 10 min. It was widely reported that the fabrication of metal oxide layers can be performed by the anodization technique in traditional alkaline electrolytes.^{22, 23} An efficient anodization process could be performed in a mixture of hydrogen peroxide-alkaline solution. An oxygen rich electrolyte was achieved due to the decomposition of H₂O₂ in the presence of the metal surface.



and



The decomposition reaction of hydrogen peroxide was reported by James *et al.*²⁴ a dark-green color was observed on the surface of the anodized thin films, which is due to the mixture of copper and cobalt oxide and hydroxide layers during the anodization. The anodization process was followed by annealing in an open tube furnace to convert the metals and metal hydroxides (dark-green) to metal oxide (black) at 500°C for 2 h. The heat treatment process for the conversion of cobalt and copper hydroxide was widely studied by Mao *et al.*, He *et al.*, and Wu *et al.*^{15, 25, 26}

Physical properties of fabricated electrodes *Structure characterizations* the structure of the fabricated thin films was characterized using X-ray diffraction technique. Figure 1 shows the FTO (red), Co₃O₄/FTO (green) and Co₃O₄-CuO/FTO (violet) diffractograms. The XRD of Co₃O₄ (green) shows the (220), (311), (400), (511) and (440) planes at 31.2°, 36.7°, 44.7°, 59.1° and 65.2°, respectively. The peaks are attributed to the cubic spinel Co₃O₄ crystal (JCPDS 42-1467). It was proven that the green layer of Co(OH)₂ from the anodization step was entirely converted to the black Co₃O₄ during the annealing process. The same phenomena were observed by Mao *et al.*, and Wang *et al.*^{15, 27} Figure 1 is the XRD of Co₃O₄-CuO/FTO (violet) where it shows the appearance the CuO planes: (110), (-111), (111), (-202), (202), (-113) and (220), and shows good agreement with the standard XRD pattern of the monoclinic CuO (ICDD-JCPS file No: 05-0661). The same results were achieved by other researchers.^{13, 28}

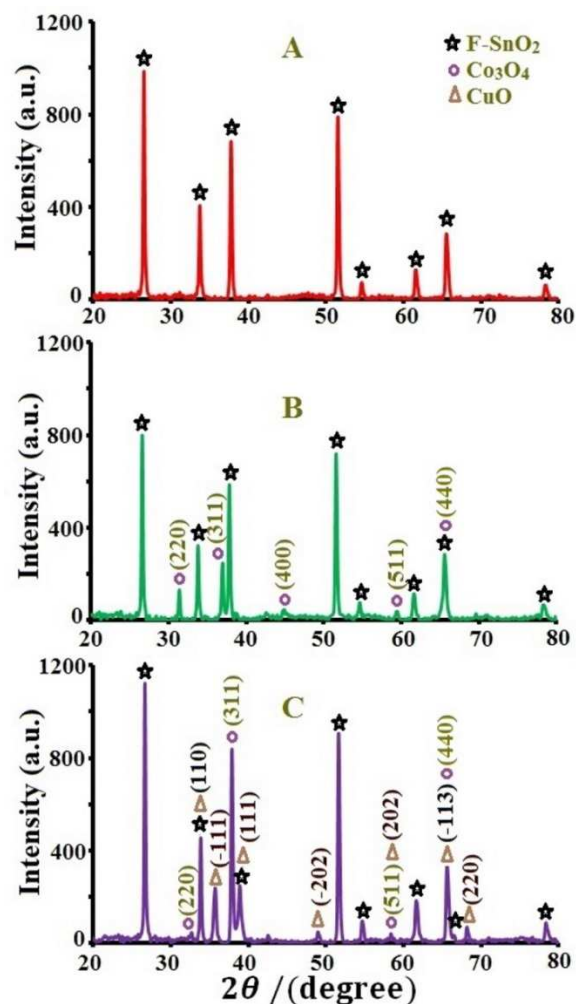


Figure 1. XRD pattern of A): FTO, B): Co₃O₄/FTO and C): Co₃O₄-CuO/FTO.

SEM/EDX studies: The cross-sectional and surface morphology of the electrodeposited/anodized and post annealed samples are shown in Fig. 2. The top view of the non-anodized and anodized (in alkaline peroxide medium) samples are displayed in Fig. 2a and 2b, for *S_B respectively. Under higher magnification (Fig. 2b), the appearance of nano-sheets can be clearly observed due to the anodization process. It was found that morphology with higher surface area can be achieved when the sample was anodized. The morphology of the sample (*S_B) is displayed in Fig. 2c. Approximately, the thickness of the prepared samples was 3 μm, the cross-sectional image of a typical sample (*S_B) is shown in Fig. 2d. Furthermore, the top view morphology of *S_C and *S_D was observed as image e and f in Fig. 2, respectively. The EDX spectrum of the samples is inserted at the corner of the corresponding image. The images show that different surface morphology can be achieved by varying the CuO content in the thin films. Interestingly, Fig. 2f shows the appearance of nano-dendrites with coconut leaf shape for *S_D (atomic%: Cu: 29.7%, Co: 10.5%, and O: 59.8%). The XRD of Fig. 2f confirms the presence of

CuO and Co₃O₄ in the thin films. The elemental compositions (EDX, %) of the thin films are tabulated in Table 1.

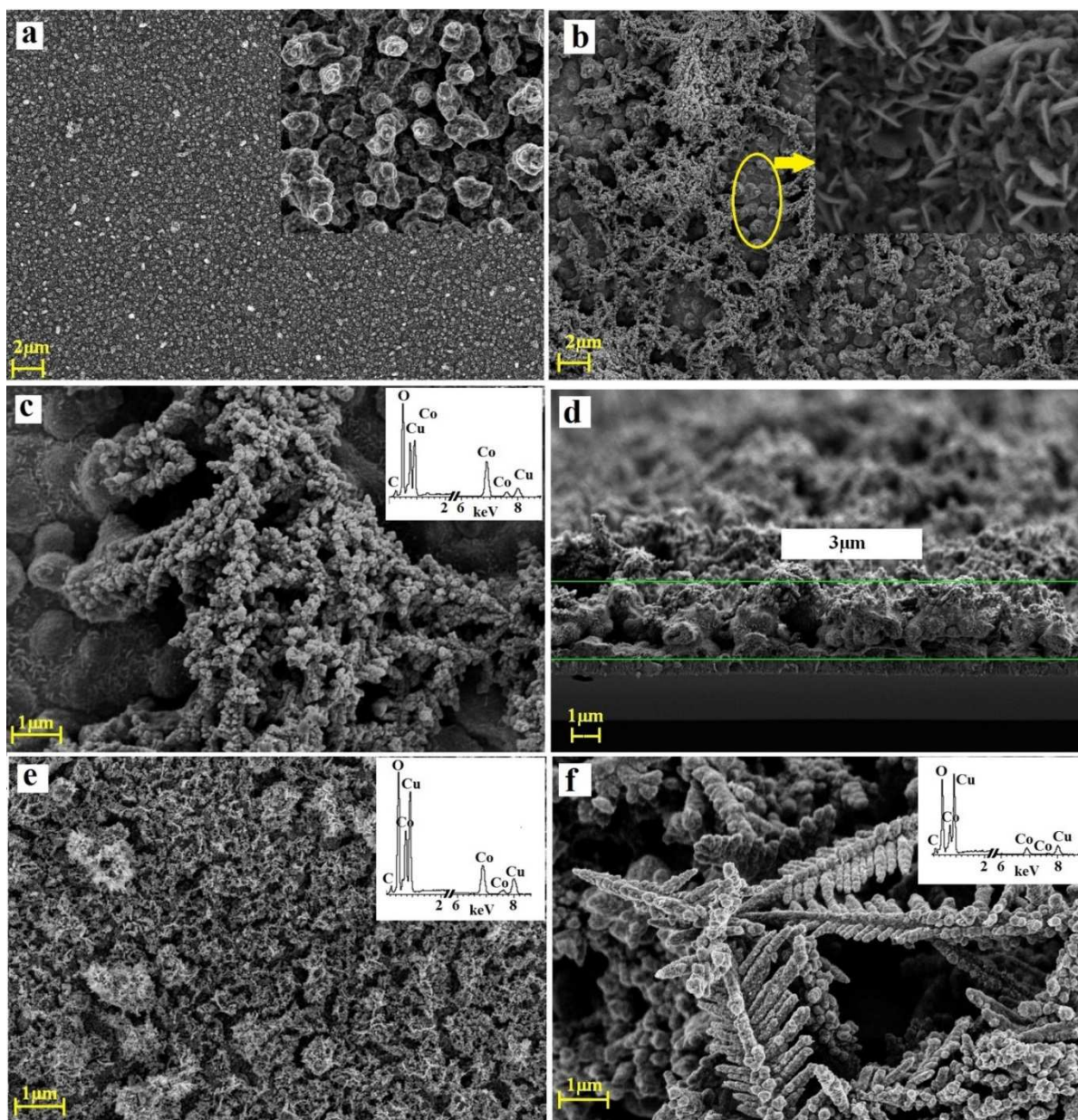


Figure 2. FESEM images of ^{*}S_B sample: a). electrodeposited layer b). Electrodeposited/annealed layer. FESEM image of prepared samples (^{*}S_B, ^{*}S_C and ^{*}S_D) via the electrodeposition/adonization/annealing process are displayed as c/d (cross-sectional view), e and f respectively.

Optical study: The optical absorption behavior of the fabricated samples was studied by UV-visible spectrophotometer in the transmission mode. As illustrated in the UV-visible spectrum, light absorption increases from the near infrared region and the band width continues to the UV region (wavelength 400 nm). Furthermore, Fig. 3a shows a red shift with the increase of CuO in the Co₃O₄ based layers. From the UV-Vis spectrum, the direct (allowed) band gap was calculated from the $(ah\nu)^2$ vs. $h\nu$ plot (Fig. 3b),²⁹

$$\alpha = \frac{\ln(10) \times A}{l} \quad (4)$$

$$\text{And } h\nu = \frac{1239.8 \text{ (eV} \times \text{nm)}}{\lambda \text{ (nm)}} \quad (5)$$

where α is the absorption coefficient, l is the thickness of the film (in this case 3 μm) and A is the absorbance.²⁹

ARTICLE

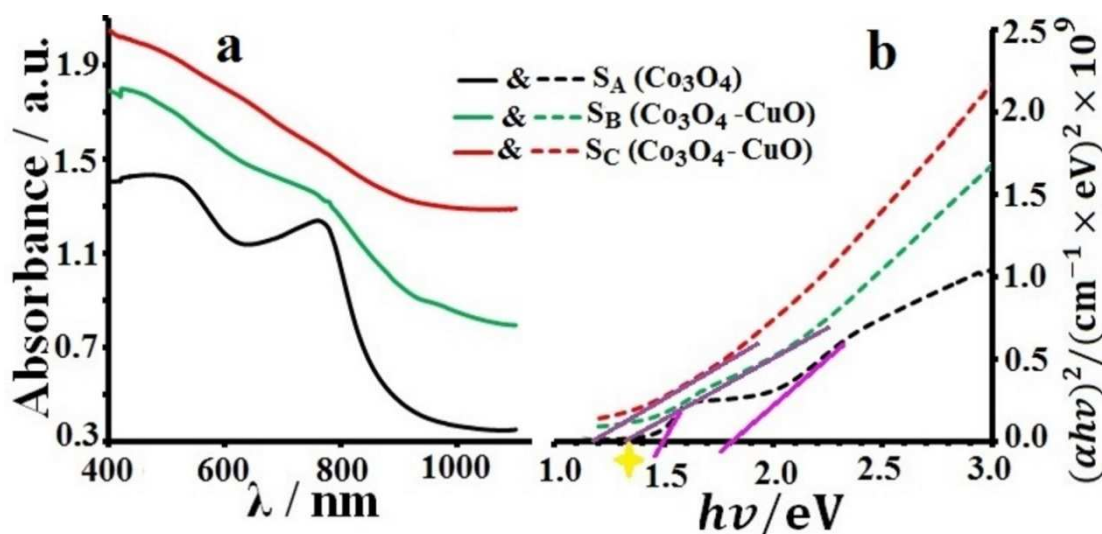


Figure 3. a). The UV-visible diffuse reflection for S_A , S_B , and S_C . b). The allowed direct band gap for the samples.

The band gap of the Co_3O_4 (S_A) was determined through the $(\alpha h\nu)^2$ vs. $h\nu$ plot, as shown in Fig. 3b. It was found that two band gap values of 1.5 and 1.8 eV were obtained via the extrapolation on the X axis. The larger band gap corresponds to a charge transfer process from the valence band of O^{2-} 2p to the conduction band of Co^{2+} 2d, and the smaller band gap is due to the charge transfer process from O^{2-} 2p to the conduction band of the Co^{3+} . These achievements are in close agreement with the literature value of Co_3O_4 .^{15, 30} The estimated band gap of S_C and S_d are 1.35 and 1.18 eV respectively, from the extrapolation on the x axis as well (Fig. 3b). It should be noted that the S_C has the higher band gap value and is closer to the ideal band energy (1.23 eV) for the water splitting process.

PEC characterization

Photocurrent investigation: The photoelectrochemical performance of the thin film electrodes was evaluated in 0.5M Na_2SO_4 between +0.3 to -0.6 V vs SCE under simulated sunlight and dark conditions (Fig. 4).

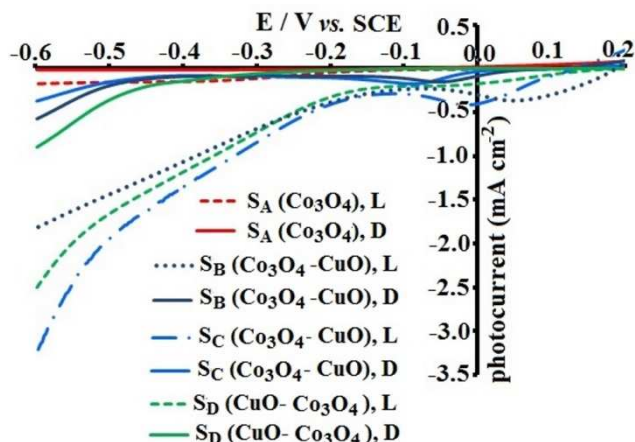


Figure 4. Current-potential curves (vs SCE) for samples Series I (S_A , S_B , S_C and S_D) from 0.2 to -0.6 V in 0.5 M Na_2SO_4 , in the absence and presence of illumination (100 mW cm^{-2}).

Figure 4 illustrates the I-V curves of the thin film samples in the dark and illuminated conditions. The performance of the thin film samples fabricated by the electrodeposition/annealing (without anodization) process were investigated by I-V plot in both dark and light conditions (Fig. 4). It was found that the current magnitude of all thin film samples increased once exposed to light. The photocurrent magnitude of the fabricated metal oxides is in the order of: $S_C > S_D > S_B > S_A$. Figure 4 demonstrates that the photocurrent was maximal when the CuO component in the Co_3O_4 thin film was optimal (atomic%: Co: 26.1, Cu: 27.3, O: 46.6). On the other hand, the photoresponse of Co_3O_4 layer (S_A) was negligible compared to

the fabricated $\text{Co}_3\text{O}_4\text{-CuO}$ samples. The poor electron transport properties of the pure Co_3O_4 are due to the lower electron excitation rate from the valence band to conducting band under illumination. Prior to the annealing process, the electrodeposited samples (Co-Cu) were anodized in an alkaline hydrogen peroxide (10%) electrolyte at 10 mA cm^{-2} (10 min). The magnitude of the photocurrent response for sample series (II) is as good as samples series (I). The analogues of Fig. 4 and Fig. 5 show that although the magnitude order of the photocurrent response are the same for both sample series, the anodized/annealed samples (series II) shows higher photocurrent value compared to the annealed samples (series I). Furthermore, as shown in Fig. 5 the photocurrent sensitivity of the prepared samples (series II) was benchmarked in the flip-flop light condition. Figure 5 illustrates that the onset of photocurrent begins from the positive potential (*vs.* SCE). In illuminated conditions, the photocurrent was maximal ($\sim 2 \text{ mA cm}^{-2}$) for $^*\text{S}_\text{C}$ sample at 0 V *vs.* SCE, whereas, the $^*\text{S}_\text{A}$ and $^*\text{S}_\text{D}$ samples gave 1.7 and 0.6 mA cm^{-2} at the same potential, respectively. Figure 5 shows that photocurrent peaks of the samples are $^*\text{S}_\text{B}$, $^*\text{S}_\text{C}$ and $^*\text{S}_\text{D}$ were slightly decreased at more negative potentials. Perhaps, this phenomenon is due to the decomposition (or electrochemical reduction) of CuO. Interestingly, it was found that the highest photocurrent ($\sim 6.5 \text{ mA cm}^{-2}$) was achieved for sample $^*\text{S}_\text{C}$ at -0.3 V . To the best of our knowledge, higher photocurrent (compared to these results) has not been reported by other cobalt oxide based electrodes in $0.5 \text{ M Na}_2\text{SO}_4$.^{7, 13, 16, 17, 25}

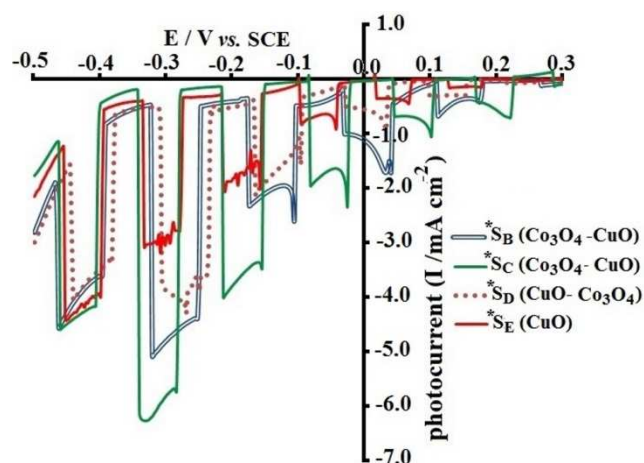
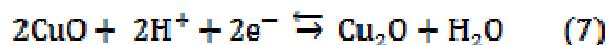
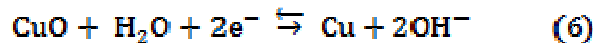


Figure 5. LSPV (I-V *vs.* SCE) in Flip-flop light (100 mW cm^{-2}) conditions for samples Series II in $0.5 \text{ M Na}_2\text{SO}_4$ from 0.3 to -0.5 V .

The photoresponse stability of the samples was benchmarked by chronoamperometry (*i-t* curves) at 0 V *vs.* SCE for 30 min in flip-flop light condition as shown in Fig. 6, where the photocurrent decays along of *i-t* curves for all samples. The photocurrent decay was approximately 50% for all examined samples (except $^*\text{S}_\text{D}$) during the initial 30 min. This fact has been also reported by other researchers as well.³¹⁻³³ The examined samples were rinsed and dried after 30 min, and it was found that the thin film color changed from grey/black to copper red during the chronoamperometry step. The same finding was reported by Sagu *et al.*, and G-Esparza *et al.*^{32, 33}

The color change is due to the electrochemical reduction of the thin films which can be described by following equations:³³



The photocurrent response of $^*\text{S}_\text{D}$ (yellow line) samples was fabricated via the electrodeposition/anodization process (without annealing). The photocurrent performance of $^*\text{S}_\text{D}$ (yellow line) is presented in Fig. 6. Among all samples, the photocurrent response of $^*\text{S}_\text{D}$ shows the poorest stability, due to the decomposition rate of metal hydroxide was faster than metal oxide samples. With regards to the color changes (from red-dark to green-red-dark) and decreasing layer thickness, equation (3) suggests that the fabricated metal hydroxide layers (by anodization) was partially reduced to $\text{M}(\text{OH})_{2(\text{ad})}$ and a fraction of that was depleted to the solution medium as $\text{M}(\text{OH})_{2(\text{aq})}$.

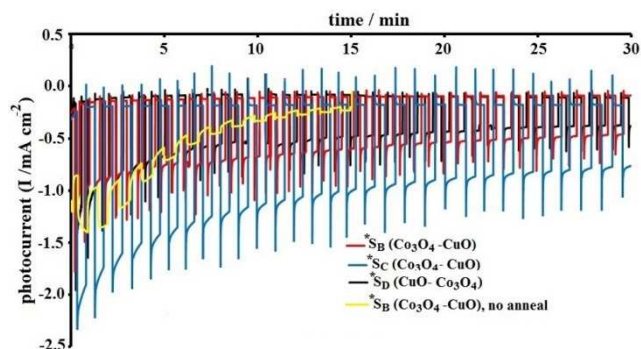


Figure 6. Photocurrent-time response of the photocathodes at 0 V *vs.* SCE under flip-flop light (100 mW cm^{-2}) condition for samples Series II in $0.5 \text{ M Na}_2\text{SO}_4$.

Electrochemical impedance measurements: EIS is a robust tool for the investigation of PEC properties which it is mostly presented by the Nyquist and Bode/Phase plots.^[29] The Nyquist plots show that the fabricated electrodes are strongly affected by illumination at 0 V (*vs.* SCE) applied potential (Fig. 7a) in the aqueous solution ($0.5 \text{ M Na}_2\text{SO}_4$). The diameter of the semicircle in the Nyquist plot shows that the overall charge transfer resistance decreases under illumination compared to the dark, for all samples. The EIS experimental data in the dark and light conditions were simulated and excellent fittings were obtained from the simulations, in the form of analog circuits³⁴ visually, the identification of the corresponding electrical analog circuit for non-ideal curves is not convenient. The equivalent electrical circuit from the EIS simulations is shown in Fig. 7b. The equivalent electrical circuit consists of two relaxation times whether in dark or light condition. As observed in Fig. 7b, both loops in the equivalent circuit are in parallel configuration. The corresponding loop of the semiconductor ($R_{\text{sc}} \parallel \text{CPE}_{\text{sc}}$) is in series with the interfacial resistance of the double layer/thin film (R_{dl}) and both of them are in parallel with the double

layer capacitance (C_{dl}). For a more accurate representation of the capacitance behavior, the constant phase element (CPE) was used instead of a pure capacitor in the simulations. The impedance of a CPE (Z_{CPE}) for a non-ideal circuit element is given as:^[34]

$$Z_{CPE} = \frac{1}{Q(j2\pi f)^n} \quad (8)$$

Where f is applied frequency, j is imaginary number, $Q = C$ if the exponent $n=1$, and $Q \neq C$ if exponent $1 > n > 0$. It must be noted that the capacitance behavior is approximated by Q , if the electrode surface is rough or when the dielectric property of the electrode components are heterogeneous.^[29] The detailed corresponding electro-kinetic elements for the samples are tabulated in Table 2. It is found that the charge transfer resistance of the semiconductor (R_{SC}) is in the order of: ${}^*S_{D(D)} > {}^*S_{C(D)} > {}^*S_{B(D)}$ in the dark, whereas, the R_{SC} value decreases in the order of: ${}^*S_{D(L)} > {}^*S_{B(L)} > {}^*S_{C(L)}$ under illumination. The LSPV (Fig. 5) correlates with the EIS results. The EIS results also emphasize that (*S_C) shows the highest efficient response to light among of all samples. It is also noted that the capacitance values (CPE_{Sc}) of the samples decreases with R_{SC} , whether in light or dark. This could be due to the decrease in the charge accumulation across the electrical double layer region when the charge transfer process becomes more prominent, and is in agreement with the deduction of Lopes *et al.*^[34]

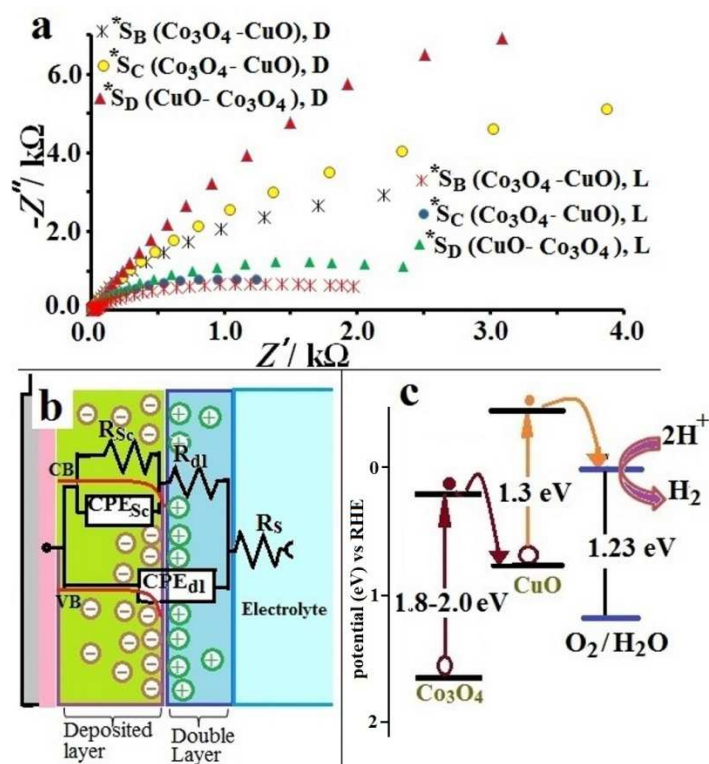


Figure 7. a): The Nyquist plots of the fabricated samples (Series II) in 0.5 M Na_2SO_4 (@ 0 V vs SCE) in the dark (D) and under illumination (L). b): energy diagram of the fabricated semiconductor/electrolyte interface with the respective electrical equivalent circuit. c): schematic representation of the heterogeneous ($\text{Co}_3\text{O}_4\text{-CuO}$) with aqueous medium in illuminated condition.

From the energy levels of the composite (Co_3O_4 , and CuO), an energy level diagram was proposed (Fig. 7c). It can be demonstrated that the PEC water splitting is enhanced due to the electron donation from the conduction band of Co_3O_4 to the valence band of CuO at low bias potentials.^[35]

Table 2. The EIS parameters from the simulation of the equivalent circuit model at bias-free potential vs SCE.

Samples	R_s (Ω)	R_{dl} (Ω)	C_{dl} (μF)	R_{sc} (Ω)	$Q(Y_o)_{sc}$ (μMho)	n
${}^*S_{B(D)}$	15.62	168.89	158.4	5303	135.52	0.78
${}^*S_{B(L)}$	11.74	10.44	11.8	2307	176.38	0.68
${}^*S_{C(D)}$	11.144	113.12	208.7	16374	339.32	0.76
${}^*S_{C(L)}$	14.874	15.467	59.9	2072	104.76	0.73
${}^*S_{D(D)}$	11.55	39.85	49.1	19290	424.82	0.81
${}^*S_{D(L)}$	10.77	33.27	11.9	3348	271.44	0.74

The space charge capacitance of the semiconductor as a function of the applied potential is represented by the Mott-Schottky equation,^[36] which leads to determination of flat band energy (E_{fb}):

$$\frac{1}{C_{sc}^2} = \frac{2}{\epsilon_r \epsilon_0 A^2 e N_D} \left(E - E_{fb} - \frac{kT}{e} \right) \quad (9)$$

where ϵ_r is the relative permittivity of the semiconductor, ϵ_0 is permittivity in vacuum, A is the surface area, e is the charge of an electron, N_D is the donor density, k is Boltzmann constant, T is the temperature, and E is the applied potential.

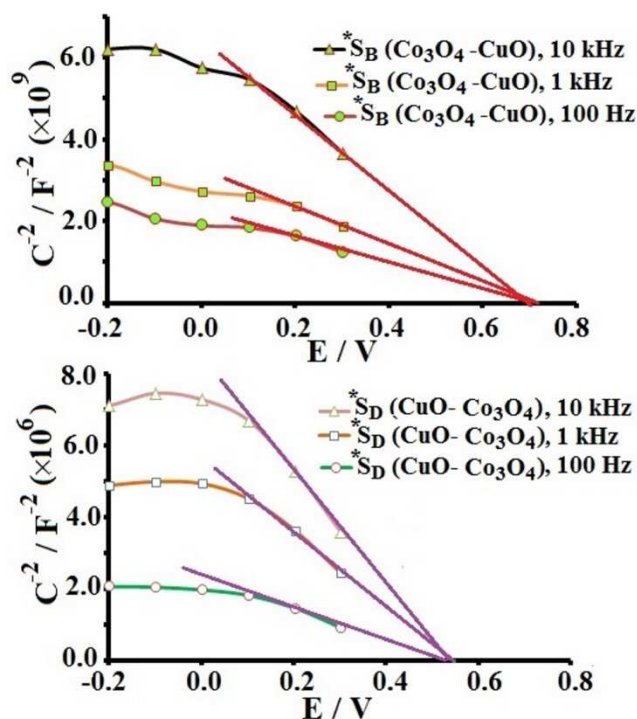


Figure 8. Mott-Schottky plots for samples ($*S_B$ and $*S_D$) in dark condition at frequencies (10, 1, 0.1 kHz).

Samples $*S_B$ and $*S_D$ were studied by M-S technique in 0.5 M Na_2SO_4 via following operation condition: potential window range (-0.2 to 0.3 V vs SCE), frequencies 1000, 100, 10 Hz, dark condition. Figure 8 shows a typical p-type behavior of fabricated semiconductors from the negative slopes of the curves at various frequencies (1000, 100 and 10). The E_{fb} for the samples was determined from the extrapolation of the slope to potential axis. The estimated E_{fb} (vs SCE) for $*S_B$ and $*S_D$ are 0.71 and 0.53 V, respectively. These values are close to the results of Zhang and Wang for CuO.³⁶

3. Conclusion

Heterogeneous Co_3O_4 -CuO photocathodes were successfully prepared via electrodeposition/ anodization (in alkaline peroxide)/ annealing in 500°C on FTO. The performance of the fabricated electrodes toward PEC was examined with LSPV, chronoamperometry, and EIS techniques. The photocurrent value

increases with the increase of CuO content in the thin films. Furthermore, the photocurrent performance of the photocathodes was enhanced with anodization in alkaline peroxide electrolyte before the annealing process. The thin films with the composition: Co: 24.9, Cu: 25.0, and O: 50.1% ($*S_C$) gave the best photocurrent performance (~ 6 and ~ 2 mA cm^{-2} vs SCE at -0.3 and 0 V, respectively). The band-gap values of the thin film samples were also determined, where the band gap of $*S_C$ was 1.35, which is suitable for hydrogen generation via the water splitting process.

Acknowledgement

The authors would like to thank the Ministry of Higher Education for the financial support from grants FRGS/2/2013/TK06/UKM/03/1 and FP033 2013A.

Notes and references

^aDepartment of Chemistry, Faculty of Science, Islamic Azad University-Gorgan Branch, Gorgan, Iran,

^{*}E-mail: mehdi_2222002@yahoo.com

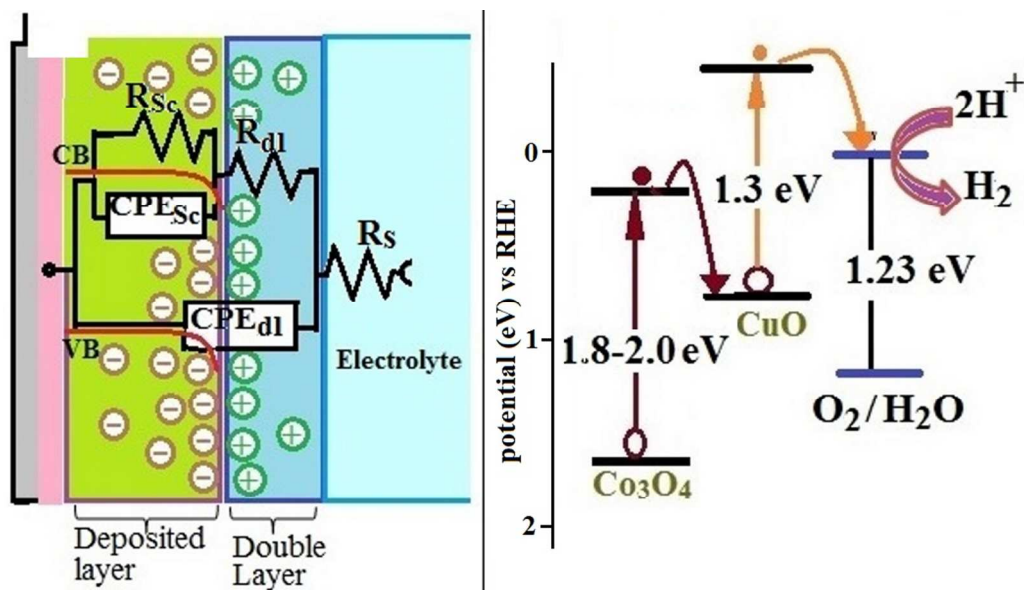
^bSolar Energy Research Institute, University Kebangsaan Malaysia, Bangi, Selangor, Malaysia.

^cDepartment of Chemistry, Faculty of Science, University of Malaya, 50603 Kuala Lumpur, Malaysia

References

- 1 M. Shao, F. Ning, M. Wei, D. G. Evans and X. Duan, *Adv. Funct. Mater.*, 2013, 24(4), 580-586.
- 2 Y. Sun, C. Liu, D. C. Grauer, J. Yano, J. R. Long, P. Yang and C. J. Chang, *Chem. Soc.*, 2013, 135, 17699-17702.
- 3 E. J. Popczun, J. R. McKone, C. G. Read, A. J. Baccchi, A. M. Wiltrout, N. S. Lewis and R. E. Schaak, *J. Am. Chem. Soc.*, 2013, 135(25), 9267-9270.
- 4 F. D. Wu and Y. Wang, *J. Mater. Chem.*, 2011, 21, 6636-6641.
- 5 C. Guan, J. P. Liu, C. W. Cheng, H. X. Li, X. G. Li, W. W. Zhou, H. Zhang and H. J. Fan, *Sci.*, 2011, 4, 4496-4499.
- 6 H. S. Jeon, W. Park, J. Kim, H. Kim, W. Kim and B. K. Min, *Int. J. Hydrogen. Energ.*, 2011, 36, 1924-e1929.
- 7 J. Chen and A. Selloni, *J. Phys. Chem. Lett.*, 2012, 3(19), 2808-2814.
- 8 T. Maruyama and T. Nakai, *Sol. Energ. Mater.*, 1991, 23(1), 25-29.
- 9 E. D. Lester, G. Aksomaityte, J. Li, S. Gomez, J. Gonzalez-Gonzalez and M. Poliakoff, *Prog. Cryst. Growth Ch.*, 2012, 58(1), 3-13.

- 10 D. Zhang, X. Li, X. Guo and C. Lai, *Mat. Letter.*, 2014, 126, 211–213.
- 11 M. S. Hill, A. L. Johnson, T. D. Manning, K. C. Molloy and B. J. Wickham, *Inorg. Chim. Acta*, 2014, 422, 47–56.
- 12 S. Choudhary, A. Solanki, S. Upadhyay, N. Singh, V. R. Satsangi, R. Shrivastav, S. Dass, *J. Solid State Electrochem.*, 2013, 17, 2531–2538.
- 13 R. Patil, S. Kelkar, R. Naphadeab and S. Ogale, *J. Mater. Chem. A*, 2014, 2, 3661–3368.
- 14 X. Yang, A. Wolcott, G. Wang, A. Sobo, R. C. Fitzmorris, F. Qian, J. Z. Zhang and Y. Li, *Nano Lett.*, 2009, 9(6), 2331–2336.
- 15 Y. Mao, W. Li, P. Liu, J. Chen and E. Liang, *Mat. Lett.*, 2014, 134, 276–280.
- 16 J. Wang and F. E. Osterloh, *J. Mater. Chem. A*, 2014, 2, 9405–9411.
- 17 L. J. Zhou, Y. Zou, G. D. Li, X. Zou, J. Zhao, M. Fan, Y. Liu and D. Wang, *RSC Adv.*, 2014, 4, 22951–22954.
- 18 J. H. Kim, S. H. Kang, K. Zhu, J. Y. Kim, N. R. Neale and A. J. Frank, *Chem. Commun.*, 2011, 47, 5214–5216.
- 19 W. Li and J. Y. Walz, *Sci. Rep.*, 2014, 4, 4418
- 20 Y. Nishijima, K. Ueno, S. Juodkazis, V. Mizeikis, H. Fujiwara, K. Sasaki and H. Misawa, *Opt. Expr.*, 2009, 17(4), 2976–2983.
- 21 G. Subramanian, V. N. Manoharan, J. D. Thorne and D. J. Pine, *Adv. Mater.*, 1999, 11(15), 1261–1265.
- 22 S. John, V. Balasubramanian and B. A. Shenoi, 1985, 26(3), 207–216.
- 23 L. Ling-ling, C. Ying-liang, W. Hui-min and Z. Zhao, *Trans. Nonferrous Met. Soc. China.*, 2008, 18, 722–727.
- 24 S. J. D. Mitchell, J. P. Farr and D. T. Carty, EP0209228 A1, 1987.
- 25 J. He, Y. Peng, Z. Sun, W. Cheng, Q. Liu, Y. Feng, Y. Jiang, F. Hu, Z. Pan, Q. Bian and S. Wei, *Electrochim. Acta*, 2014, 119, 64–71.
- 26 X. Wu, H. Bai, J. Zhang, F. Chen and G. Shi, *J. Phys. Chem. B*, 2005, 109, 22836–22842.
- 27 X. Wang, X. Dong, Y. Wen, C. Li, Q. Xiong and P. Chen, *Chem. Commun.*, 2012, 48, 6490–6492.
- 28 W. Wang, L. Wang, H. Shi and Y. Liang, *Cryst. Eng. Comm.*, 2012, 14, 5914–5922.
- 29 Z. Chen, H. N. Dinh and E. Mille, *Springer New York Heidelberg Dordrecht London*, 2013.
- 30 F. Gu, C. Li, Y. Hu and L. Zhang, *J. Cryst. Grow*, 2007, 304(2), 369–373.
- 31 A. Paracchino, V. Laporte, K. Sivula, M. Grätzel and E. Thimsen, *Nat. Mater.*, 2011, 10, 456–461.
- 32 J. S. Sagu, T. A. Nirmal Peiris and K.G. UpulWijayantha, *Electrochem. Commun.*, 2014, 42, 68–71.
- 33 A. T. Garcia-Esparza, K. Limkraisiri, F. Leroy, S. Rasul, W. Yu, L. Lin and K. Takanebe, *J. Mater. Chem. A*, 2014, 2, 73–89.
- 34 T. Lopes, L. Andrade, H. A. Ribeiro and A. Mendes, *Int. J. Hydrogen. Energ.*, 2010, 35, 11601–1608.
- 35 J. Barber and P. D. Tran, *J. Roy. Soc. Interf.*, 2013, 81(10), 5689–5662.
- 36 Z. Zhang and P. Wang, *J. Mater. Chem.*, 2012, 22, 24–56.

Graphical Abstract:

Highlight: Electrofabricated p- Co_3O_4 based electrodes have shown the efficient photoelectrochemical performance at low bias potentials in aqueous medium ($\sim 6.5 \text{ mA cm}^{-2}$ vs SCE at -0.3 V).